Brain Research 1735 (2020) 146717

Contents lists available at ScienceDirect

Brain Research

journal homepage: www.elsevier.com/locate/brainres

Research report

Defining the adult hippocampal neural stem cell secretome: In vivo versus in vitro transcriptomic differences and their correlation to secreted protein levels

Jiyeon K. Denninger[a], Xi Chen[b], Altan M. Turkoglu[c], Patricia Sarchet[b], Abby R. Volk[c], Joshua D. Rieskamp[d], Pearlly Yan[b,e], Elizabeth D. Kirby[a,f,g,*]

[a] Department of Psychology, College of Arts and Sciences, The Ohio State University, United States
[b] Comprehensive Cancer Center, The Ohio State University, United States
[c] College of Arts and Sciences, The Ohio State University, United States
[d] Neuroscience Graduate Program, The Ohio State University, United States
[e] Division of Hematology, Department of Internal Medicine, College of Medicine, The Ohio State University, United States
[f] Department of Neuroscience, The Ohio State University, United States
[g] Chronic Brain Injury Initiative, The Ohio State University, United States

HIGHLIGHTS

- The neural stem and progenitor cell (NSPC) secretome is currently undefined.
- In vitro NSPC intracellular and secreted proteins were assessed by array and LC-MS/MS.
- Gene expression does not reliably predict secreted protein abundance in vitro.
- Gene expression profiles of in vitro and in vivo NSPCs strongly correlate.
- Combined protein and RNA level analysis of in vivo and in vitro NSPCs is needed.

ARTICLE INFO

Keywords:
Neural stem cell
Secretome
Conditioned media
BONCAT
RNA sequencing

ABSTRACT

Adult hippocampal neural stem and progenitor cells (NSPCs) secrete a variety of proteins that affect tissue function. Though several individual NSPC-derived proteins have been shown to impact key cellular processes, a broad characterization is lacking. Secretome profiling of low abundance stem cell populations is typically achieved via proteomic characterization of in vitro, isolated cells. Here, we identified hundreds of secreted proteins in conditioned media from in vitro adult mouse hippocampal NSPCs using an antibody array and mass spectrometry. Comparison of protein abundance between antibody array and mass spectrometry plus quantification of several key secreted proteins by ELISA revealed notable disconnect between methods in what proteins were identified as being high versus low abundance, suggesting that data from antibody arrays in particular should be approached with caution. We next assessed the NSPC secretome on a transcriptional level with single cell and bulk RNA sequencing (RNAseq) of cultured NSPCs. Comparison of RNAseq transcript levels of highly secreted proteins revealed that quantification of gene expression did not necessarily predict relative protein abundance. Interestingly, comparing our in vitro NSPC gene expression data with similar data from freshly isolated, in vivo hippocampal NSPCs revealed strong correlations in global gene expression between in vitro and in vivo NSPCs. Understanding the components and functions of the NSPC secretome is essential to understanding how these cells may modulate the hippocampal neurogenic niche. Cumulatively, our data emphasize the importance of using proteomics in conjunction with transcriptomics and highlights the need for better methods of unbiased secretome profiling.

* Corresponding author.
E-mail address: kirby.224@osu.edu (E.D. Kirby).

https://doi.org/10.1016/j.brainres.2020.146717
Received 5 September 2019; Received in revised form 3 February 2020; Accepted 5 February 2020
Available online 06 February 2020

1. Introduction

In the adult mammalian brain, neural stem cells (NSCs) are located in two specific niches, the subventricular zone (SVZ) and the subgranular zone (SGZ) of the hippocampal dentate gyrus (DG) (Gage and Temple, 2013). In the adult SGZ, resident radial glia-like NSCs (RGL-NSCs) produce intermediate progenitor cells (IPCs) that proliferate throughout the lifespan of the organism to produce functionally-relevant neurons and astrocytes (Ming and Song, 2011). In addition to creating mature cell types, NSCs also secrete an array of growth factors and cytokines, collectively termed the stem cell secretome (Drago et al., 2013; Bacigaluppi et al., 2020). In the healthy adult SGZ, RGL-NSCs and their progenitors (together NSPCs) have been shown to produce the secreted factors milk-fat globule EGF-factor 8 (MFGE8) and vascular endothelial growth factor (VEGF), both of which regulate NSPC maintenance through autocrine signaling (Kirby et al., 2015; Zhou et al., 2018), as well as pleitrophin (PTN) which drives maturation of immature, developing neurons (Tang et al., 2019). However, while the secretome of other tissue stem cells, such as mesenchymal stem cells, has been extensively catalogued (Liang et al., 2014; Teixeira and Salgado, 2020), a comprehensive characterization of the NSPC secretome is lacking (Andres et al., 2011; Ryu et al., 2004; Yasuhara et al., 2006; Ourednik et al., 2002; Tang et al., 2019; Bacigaluppi et al., 2020).

Protein-level analysis of the stem cell secretome is typically accomplished using in vitro models, where the conditioned media (CM) of isolated stem cells is profiled using proteomics approaches such as antibody-based arrays or liquid chromatography-tandem mass spectrometry (LC-MS/MS). While these approaches have provided the first broad understanding of the content and variety of several tissue stem cell secretomes (Skalnikova et al., 2011), they are limited by two main factors: 1) in the case of arrays, the scope and specificity of the pre-selected antibodies present on the arrays and 2) in both cases, potential differences in protein production in in vitro versus in vivo systems.

Commercial antibody arrays are thus far the most common method for secretome identification because the arrays can contain antibodies for hundreds to thousands of proteins and can be used with CM from standard culture conditions, including those with high levels of serum-derived protein supplements. However, the list of potentially detected targets is still confined to the pre-identified targets and specificity of those hundreds to thousands of antibodies can be impractical to verify. LC-MS/MS, in contrast, can yield a more unbiased identification of proteins in CM with less likelihood of false signals than antibody arrays, but traditionally requires serum deprivation of cells to detect cell-secreted proteins. Serum deprivation can dramatically disrupt numerous cell processes and change the secretome (Pirkmajer and Chibalin, 2011).

While the issue of culture-induced change in protein secretion is particularly severe when serum deprivation is required as with LC-MS/MS, it can also be problematic when studying the secretome in standard culture conditions. Comparison of cultured cells to their in vivo counterparts in several organ systems has provided increasing evidence of significant changes that occur when cells are transitioned from an in vivo to an in vitro environment (Durr et al., 2004; Binato et al., 2013; Duggal et al., 2009). These changes are dependent both on the method of isolation (Wernly et al., 2017) and the conditions of culture maintenance (Shahdadfar et al., 2005; Duggal and Brinchmann, 2011). More specific to NSPCs, key differences in gene expression of inflammatory and cytokine signaling factors were identified between in vitro SVZ NSCs versus in vivo NSCs freshly isolated from the SVZ (Dulken et al., 2017).

The potential hazards of in vitro analysis of stem cell secretomes suggest that in vivo approaches might be superior. However, high-throughput characterization of tissue stem cell secretomes in vivo faces several challenges as well. In vivo, adult tissue stem cells, including hippocampal NSPCs, are small populations residing in heterogeneous niches, which impedes the sufficient isolation of cells necessary for most large-scale proteomics protocols. Methods such as immunostaining of tissue sections or flow cytometry of dissociated cells allow detection of pre-selected proteins in specific cells, but are limited in the total number and type of proteins that can be examined in each instance. To broaden the scope of in vivo protein investigation, extracellular factors can be identified from tissue niches with high performance liquid chromatography (HPLC) or mass spectrometry of microdialysates. However, these methods fail to determine the cells that produce the secreted factors. In contrast to proteomic approaches, high throughput RNA sequencing (RNAseq) is adaptable to low cell input and several studies have recently provided large-scale quantification of gene expression in acutely isolated NSPCs by single cell RNAseq (scRNAseq) (Hochgerner et al., 2018; Shin et al., 2015; Artegiani et al., 2017; Dulken et al., 2017; Zywitza et al., 2018). However, transcriptional activity does not always correlate well with bioavailable protein due to added layers of regulation on post-transcriptional and post-translational levels (Lipshitz et al., 2017; Besse and Ephrussi, 2008).

Given that mRNA levels may not reflect secreted protein levels and in vitro gene expression may not mirror in vivo expression, we chose to create a multi-faceted analysis of the adult hippocampal DG NSPC secretome from mRNA level to secreted protein of in vitro cultured NSPCs. For high-throughput protein-level quantification, we used a protein array to probe for over 300 different cytokines and growth factors secreted by cultured adult hippocampal NSPCs. Furthermore, we performed unbiased LC-MS/MS based analyses of in vitro NSPC intracellular and secreted proteins. Secreted proteins were identified without any supplement deprivation by using biorthogonal non-canonical amino acid tagging (BONCAT) of newly synthesized proteins to select and enrich for proteins synthesized by NSPCs in the CM (Dieterich et al., 2006). We next compared these protein-level data with transcriptional-level data derived from bulk and single cell RNAseq of similarly maintained in vitro NSPCs to reveal the potential relationship between transcriptional expression and protein expression and secretion. Last, to evaluate the equivalence of in vitro and in vivo NSPCs, we examined two independently published single cell sequencing datasets of endogenous, in vivo hippocampal NSPCs (Shin et al., 2015; Hochgerner et al., 2018). Comparison of all these datasets demonstrated important divergence between transcriptional and translational expression, and also an overall agreement between cultured and in vivo hippocampal NSPC transcriptional expression. Our findings therefore not only provide a broad characterization of the putative adult DG NSPC secretome, but also highlight the need to consider limitations of currently available methods for secretome profiling.

2. Results

2.1. Protein array of cultured adult hippocampal NSPC conditioned media detects several secreted factors that may impact NSPC function

Adult hippocampal NSPC cultures were established from male and female C57BL/6J mice (n = 4 mice per line) and maintained according to previously published methods (Babu et al., 2011; Kirby et al., 2015). As expected, when maintained in proliferative conditions, these cultures showed immunoreactivity for NSPC markers NESTIN, GFAP, and Ki67 (Fig. 1A) and when under differentiating culture conditions, they generated β3-Tubulin$^+$ neurons and S100β$^+$ astrocytes (Supplemental Fig. 1A–D). To further examine the NSPC phenotype of these cells, four separate cultures of adult hippocampal NSPCs (two male and two female) were harvested and analyzed by bulk RNA sequencing. Over 25,000 unique transcripts were detected (Supplemental Table 1). Examination of known transcriptional markers for quiescent RGL-NSCs (qRGLs), activated RGL-NSCs (aRGLs), and IPCs indicated that cultured NSPCs mainly consisted of quiescent and activated RGL-NSCs (Fig. 1B) (Shin et al., 2015; Hochgerner et al., 2018). These subpopulations were confirmed with single cell (sc)RNAseq on 14,912 cultured NSPCs from three independent passages of cells. Unsupervised clustering analysis of

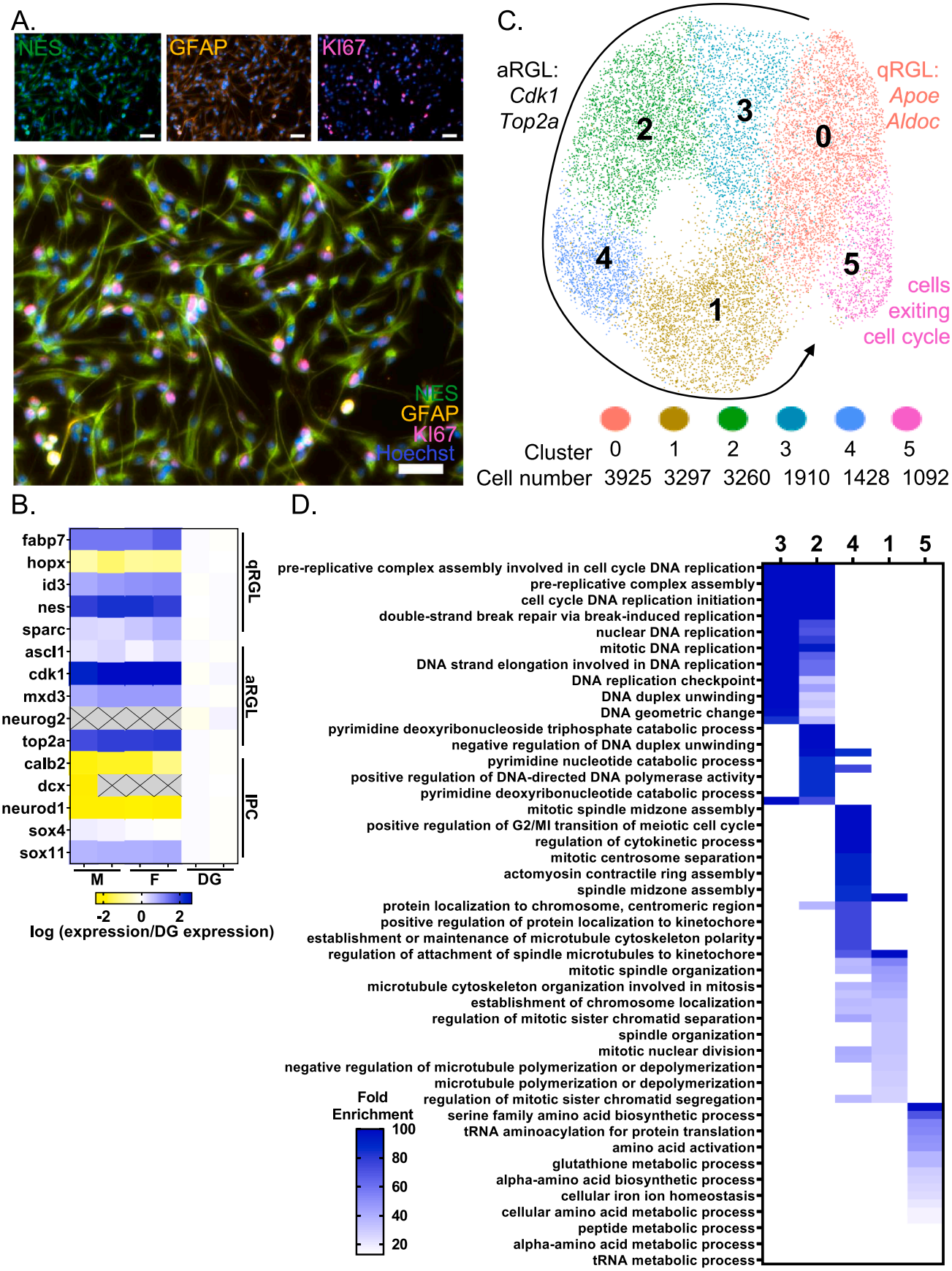

Fig. 1. Characterization of in vitro cultured NSPCs. (A) Immunofluorescent staining of known NSPC markers NESTIN, GFAP, and KI67. (scale bar = 50 μm) (B) Heatmap of log fold change of gene length normalized transcript expression in NSPCs over whole DG expression from bulk RNAseq of cultured NSPCs and whole DG. (C) tSNE plot of clustering analysis for scRNAseq of cultured NSPCs. (D) Heatmap of fold enrichment values for top 20 GO biological process terms from differentially expressed genes defining each scRNAseq cluster.

the transcriptional data was visualized on a t-distributed stochastic neighbor embedding (t-SNE) plot which yielded 6 clusters that were all enriched for markers of RGL-NSCs such as *Nestin* and *Fabp7* (Fig. 1C and Supplemental Fig. 1E). Several clusters of cells showed high expression of gene markers for aRGLs such as *Cdk1* and *Top2a*, and one cluster (cluster 0) showed enrichment for markers associated with qRGLs, such as *Apoe* and *Aldoc* (Supplemental Fig. 1E). These data indicated that NSPC cultures consisted mainly of quiescent and activated NSCs (Fig. 1B and C). GO term analysis of differentially expressed genes (DEGs) between the clusters revealed that the clusters appeared to separate most strongly based on stages in cell cycle (Fig. 1D, Supplemental Table 2). Specifically, biological process GO term enrichment revealed a progression counterclockwise from group 3 to 2 to 4 to 1 with DEGs associated with DNA synthesis to mitotic spindle assembly to chromosome segregation and separation, and finally to mitosis and cytokinesis. These data suggested that groups 3, 2, 4, and 1 represented activated NSCs as they progressed through cell cycle phases: G_1, S, G_2, mitosis, and cytokinesis (Supplemental Fig. 1F). Group 5 DEGs were enriched for GO terms associated with several aspects of translation and possibly represents early IPCs, as translation processes have been shown to be upregulated at this phase of differentiation (Shin et al., 2015).

To provide an initial assessment of the secretome derived from these cultured NSPCs, conditioned media (CM) from three separate adult hippocampal NSPC cultures (one male and two female) were collected and probed for over 300 growth factors, cytokines, chemokines, adipokines, angiogenic factors, proteases, soluble receptors and soluble adhesion molecules with a protein antibody array. Supplemental Table 3 lists the fluorescence values after normalization to average fluorescence intensity within each slide for all factors that were detected in the assay ranked by Z-score. Of these, the top 50 most highly detected factors were selected for further scrutiny (Fig. 2A). One of the top intensity factors was vascular endothelial growth factor (VEGF), which we previously identified as highly secreted by NSPCs and critical for stem cell maintenance in vivo and in vitro (Kirby et al., 2015). In addition, many other soluble growth factors and cytokines showed high signal intensity, along with several carrier proteins that are implicated in NSPC maintenance such as those of the IGFBP family (IGFBP-3, IGFBP-2, and IGFBP-5) (Kalluri and Dempsey, 2011; Shen et al., 2019; Barkho et al., 2006). Soluble fragments of receptors that promote NSPC maintenance and proliferation, such as TYRO3, were also found, possibly reflecting shedding of the extracellular portions from these typically membrane-integral receptors (Ji et al., 2014). Known regulators of apoptosis that promote NSPC survival, FAS and SPP1, were also detected in the top 50 signals (Knight et al., 2010; Rabenstein et al., 2015). CD70 on NSPCs, shown to interact with CD27 on $CD4^+$ T-cells to induce FAS-mediated apoptosis of T cells, was also detected (Lee et al., 2013). Cumulatively, the protein array indicated the presence of several previously reported components of the NSPC secretome and suggested numerous other potentially bioactive proteins produced and secreted by these cells.

Given the potential for non-specific binding in the antibody array, ELISAs were used to verify and quantify select individual proteins. CM and cell lysates were generated from three different NSPC cultures, one male and two female (n = 3 per line), and probed for 3 of the top 5 proteins identified in the array, VEGF, LIF, and IGFBP-2, as well as one protein that was detected very lowly on the array and was not part of the top 50 factors, FASL (Fig. 2B and C). As previously published, VEGF was detected in both NSPC CM and NSPC cell lysate (Fig. 2B and C). IGFBP-2 was also detected in CM and lysate but at over 10-fold higher levels than VEGF in the same media despite showing slightly lower intensity value than VEGF in the array (Fig. 2A–C). Although LIF was the fourth highest ranked factor on the antibody array, LIF was not detected in CM or cell lysate, but lysate-derived LIF was near the threshold of detection by ELISA, suggesting low levels of LIF expression in these cells (Fig. 2B and C). Interestingly, while FASL, ranked 260th on the array, was not detected in the CM by ELISA, it was readily detected in NSPC cell lysates by ELISA, suggesting that NSPCs do synthesize FASL, but that levels in the CM did not reach array or ELISA threshold (30 pg/ml) (Fig. 2B and C). These comparisons of protein levels detected in the ELISA with that suggested by the antibody array imply that this array may be frequently inaccurate at quantifying relative proteins amounts, likely due to variations in efficiency or specificity of target binding by antibodies.

2.2. Semi-quantitative LC–MS/MS of NSPC produced proteins enables unbiased identification of NSPC secreted proteins

To circumvent the limitations of antibody-based protein detection methods, we next pursued unbiased identification of NSPC-produced proteins using LC-MS/MS. First, we harvested cell lysates from two male and two female cultured NSPCs and used the exponentially modified protein abundance index (emPAI) derived from LC-MS/MS spectral counts of peptides to determine the relative level of proteins (Supplemental Table 4) (Shinoda et al., 2009; Ishihama et al., 2005). Approximately 4000 unique proteins were identified in NSPC lysates. Four of the LC-MS/MS identified proteins, IGFBP-3, IGFBP-2, GRN, and COL18A1, were also among the top 50 secreted proteins in the array of CM (Supplemental Fig. 2). However, most of the top 50 array proteins were not detected in NSPC lysates by LC–MS/MS. Expanding the comparison to all of the factors on the antibody array still only yields an additional eight proteins identified by LC–MS/MS: EGFR, SPARC, ALCAM, TR10B (TRAIL2, TNFRSF10B), MFGE8, β-Catenin (CTNB1), CSK, and F3. However, secreted proteins are frequently present in only low levels intracellularly because of constant secretion to the extracellular environment. Lack of detection of a secreted protein in cell lysate therefore is an inconclusive measure of its relative abundance in the secretome.

To examine NSPC-secreted proteins, we chose to use LC–MS/MS-based semi-quantitative analysis of NSPC CM. A major challenge of MS-based analysis of culture CM in many cell systems is high levels of exogenously-supplied proteins from serum supplements. While NSPC culture does not use animal serum, it does contain large amounts of defined protein supplements, particularly fatty acid free fraction V of bovine serum albumin. LC–MS/MS of CM containing this supplement would have limited resolution for identifying NSPC-derived proteins because of the large amounts of supplement-derived protein. One method to circumvent this problem is to supplement-deprive the cells before collecting CM. However, deprivation protocols can dramatically alter cell physiology in vitro (Pirkmajer and Chibalin, 2011). Therefore, we chose to use biorthogonal non-canonical amino acid tagging (BONCAT) (Dieterich et al., 2006) to label newly synthesized proteins in standard culture conditions and then enrich for them before LC-MS/MS. In this method, cultures are pulsed with azidohomoalanine (AHA), a non-canonical amino acid bearing an azide moiety, that is incorporated by cells into nascent proteins instead of methionine. Presence of AHA in the amino acid chain of a protein therefore serves as a marker of a newly synthesized protein (i.e. one not derived from culture supplements). Azide groups in AHA, which are biologically rare, can undergo click chemistry reactions with similarly biologically rare alkyne groups to enable their visualization or selection (Jewett and Bertozzi, 2010). In the present experiments, we pulsed cultured NSPCs with AHA and then used magnetic beads functionalized with dibenzocyclooctyl (DBCO), which undergoes a strain promoted alkyne-azide cycloaddition reaction spontaneously. The bound proteins were then digested off of the beads before LC-MS/MS analysis. In sum, this method allowed for enrichment of NSPC-derived proteins for their subsequent unbiased identification via LC–MS/MS (Rothenberg et al., 2018).

While BONCAT has been successfully applied to in vivo mature neuronal populations (Alvarez-Castelao et al., 2019), it has yet to be applied to adult NSPCs. We therefore first performed several

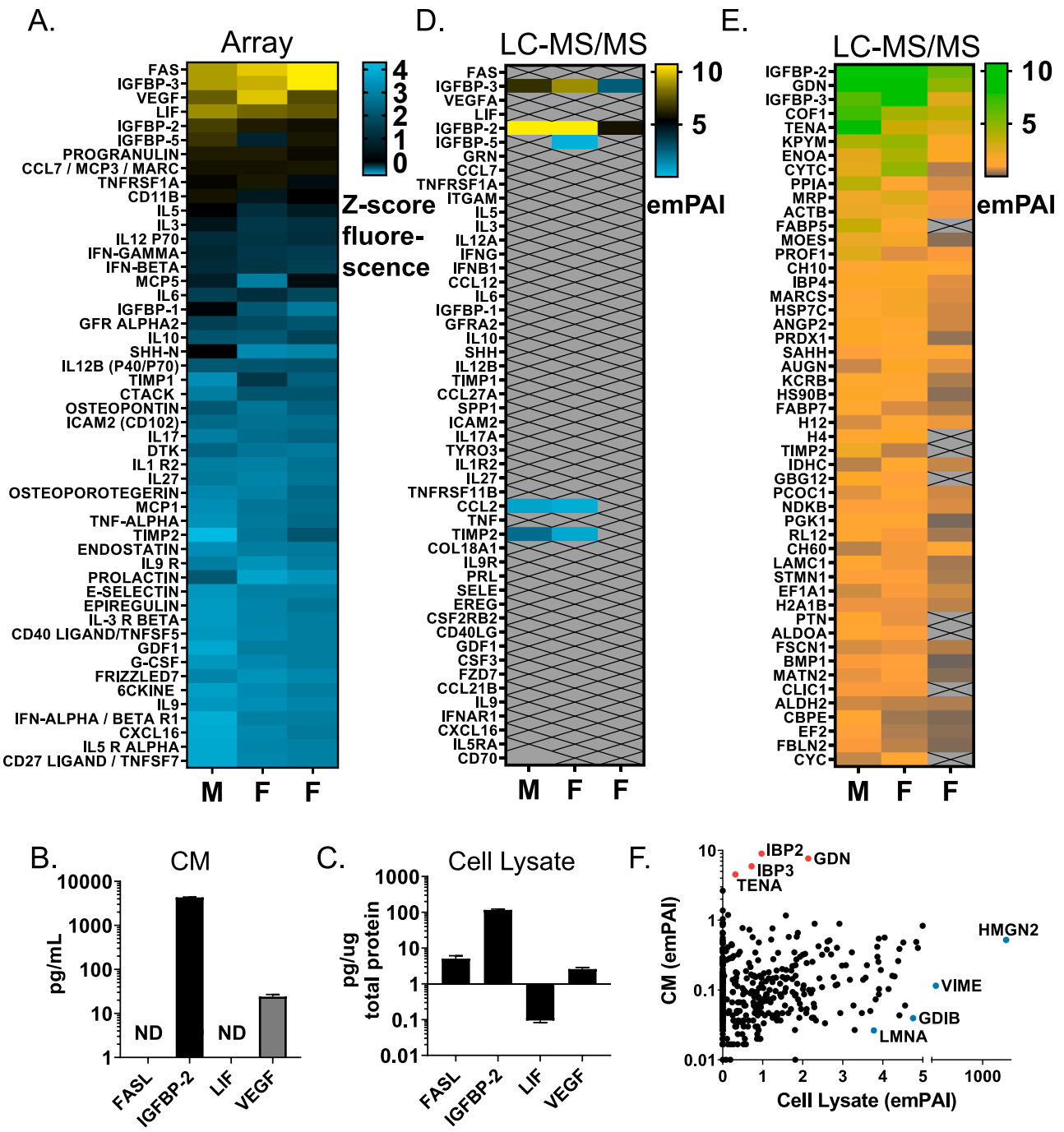

Fig. 2. Secretome analysis in cultured NSPCs. (A) Heatmap of top 50 protein signals in NSPC CM by array. Data normalized to average fluorescence intensity within each slide before Z-score transformation. (M = male, F = female). (B) ELISA quantification of FASL, IGFBP-2, LIF, and VEGFA in NSPC CM (n = 3). (C) ELISA quantification of FASL, IGFBP-2, LIF, and VEGFA in NSPC cell lysate (n = 3). (D) Heatmap of emPAI values determined by LC-MS/MS of BONCAT-enriched proteins from NSPC CM for the top 50 antibody array factors and the top 50 factors from LC-MS/MS emPAI quantification (E). X means protein not identified in CM by LC-MS/MS. (F) Correlation of emPAI values for proteins identified by LC-MS/MS in NSPC CM and NSPC cell lysate. (M = male, F = female).

preliminary experiments to develop an AHA administration protocol that tagged proteins without altering NSPC physiology. Base NSPC growth medium contains a supraphysiological amount (> 200 μM) of methionine which prevents the competitive substitution of AHA in to growing peptide chains. Thus, we cultured NSPCs with methionine-depleted growth media supplemented with fixed amounts of methionine and AHA to determine optimal concentrations that enabled maximal detection of AHA without compromising cell physiology (Supplemental Fig. 3A). NSPCs treated with varying doses of AHA and methionine were assessed for viability and proliferation by Hoechst staining and BrdU incorporation which indicated that as low as 12.5 μM methionine could maintain cell proliferation at similar levels to the standard methionine levels in NSPC culture and that AHA doses up to 200 μM did not alter proliferation (Supplemental Fig. 3B and C). Quantification of AHA intensity by reaction with a DBCO-IR800 dye and subsequent quantitative in-cell imaging revealed that 100 μM AHA would yield robust tagging of new proteins (Supplemental Fig. 3D). At 12.5 μM methionine and 100 μM AHA, there was no difference in the amount of VEGF protein secreted by NSPCs treated with AHA versus vehicle control, providing another piece of evidence that AHA

treatment did not grossly alter cell physiology or protein secretion (Supplemental Fig. 3E).

Using the conditions defined above, one male and two female independent cultures of NSPCs were treated for 24 h with AHA or vehicle. DBCO-conjugated magnetic beads were then used to enrich for tagged proteins which were subsequently identified by LC-MS/MS (Supplemental Table 5). Of the protein supplements provided in NSPC culture media, only albumin and catalase were detected as non-NSPC-derived signals among bead-digested peptides. A Wilcoxon ranked sum comparison of emPAI normalized to albumin confirmed that bead enrichment of AHA tagged proteins was successful, resulting in a two-fold increase in protein capture compared to vehicle controls (Supplemental Fig. 3F). Of the top 50 proteins identified in the antibody array, five were also detected in the NSPC CM by LC-MS/MS, namely IGFBP-3, IGFBP-2, IGFBP-5, CCL2, and TIMP2 (Fig. 2D). However, most of the proteins from the antibody array top 50 were again absent in the LC-MS/MS identified proteins. Expanding the analysis to the lower expressed proteins on the antibody array yielded an additional five proteins that were detected in LC-MS/MS: Fractalkine (CX3CL1), VEGFC, TIMP4, MFGE8, and IGFBP-7 (IBP7). Fig. 2E shows the top 50 secreted proteins identified by LC-MS/MS in AHA-enriched samples, revealing many additional, abundantly secreted proteins not assessed on the array.

To further validate production of proteins detected in CM by NSPCs, LC-MS/MS identified proteins from CM were compared to proteins from cell lysate. Strong correlation between secreted and intracellular proteins was found ($r(3\ 0\ 8) = 0.4733$, $p < 0.0001$) with most of the proteins detected in NSPC CM also detected in NSPC cell lysate (Fig. 2F). Notably, VEGFA, which was detected in the antibody array and confirmed with ELISA, was absent not only from LC-MS/MS of NSPC CM, but also from LC-MS/MS of NSPC cell lysate (Fig. 2A–C and Supplemental Tables 4 and 5). These data suggest that, as might be expected, LC-MS/MS has somewhat limited sensitivity, and emphasizes that absence of a protein in LC-MS/MS of CM does not necessarily mean a protein is not secreted in meaningful amounts. However, the relative dearth of LC-MS/MS confirmed proteins among the highest signal proteins in the array does suggest that the array does not provide accurate estimates of relative protein amount for many of its targets.

2.3. RNA sequencing of in vitro cultured NSPCs reveals that transcriptional expression can substantially deviate from relative protein levels of secreted factors

Extending our analysis of the secretome to the transcriptional level, we assessed relative mRNA expression via bulk RNA sequencing described in Fig. 1B. Gene-length normalized transcript counts from cultured NSPCs for the genes that encode the top 50 secreted factors identified in the antibody array revealed that the majority of the array top 50 protein factors from CM were not highly transcribed at the mRNA level (Fig. 3A). Almost half of the factors were not detected in any of the samples, implying either transcript expression that is below the threshold for detection by RNAseq or false positive detection in the protein array. To evaluate the relationship between mRNA levels and protein abundance, Spearman correlation analysis of relative protein levels versus length-normalized transcript levels from cultured NSPCs for the top 50 antibody array factors was performed, which showed a moderate degree of correlation overall ($r(31) = 0.3904$, $p = 0.0299$) (Fig. 3B). Though some factors, such as *Igfbp3* and *Igfbp2* (displayed in purple), displayed relatively high levels of both transcript and secreted protein detected in the CM array, several factors, such as *Fas, Vegfa*, and *Lif* (displayed in blue) or *Col18a1* and *Ifnar1* (displayed in red) respectively, showed unexpectedly low or high transcriptional expression for their ranking in the array. scRNAseq also demonstrated high and uniform expression by all clusters of cultured NSPCs for the highly secreted factors *Igfbp3* and *Igfbp2* (Supplemental Fig. 4A). Several of the transcripts were further investigated with real time quantitative reverse transcription-PCR (qrt-PCR) (Supplemental Fig. 4B-C). For *Igfbp3*, *Igfbp2*, and *Col18a1*, qrt-PCR confirmed RNAseq findings of high relative transcript levels (Supplemental Fig. 4B). qrt-PCR also corroborated very low transcript levels of *Fasl and Icam2*, which were not detected by RNAseq. These lower levels were not due to sub-optimal primer design as positive controls amplified at levels comparable with highly transcribed genes (Supplemental Fig. 4C). For *Vegf*, which showed unexpectedly lower transcript levels by bulk RNAseq, qrt-PCR actually showed comparable levels of transcript with *Igfbp3* and *Igfbp2*.

Length-normalized transcript levels from bulk RNAseq of cultured NSPCs for the top 50 NSPC secreted proteins identified by LC-MS/MS revealed better overall agreement between transcript and protein level expression than that for the array top 50, with high transcript expression being evident for the majority of the top 50 LC-MS/MS identified proteins (Fig. 3C). To better determine whether mRNA predicts relative protein abundance, Spearman correlation analysis between all secreted NSPC factors identified by LC-MS/MS of CM and RNAseq length-normalized transcript count from cultured NSPCs was performed. This comparison also showed a only moderate degree of correlation ($r(435) = 0.3824$, $p < 0.0001$) (Fig. 3D), implying that even with an unbiased LC-MS/MS approach to protein identification, RNA transcript levels can deviate from relative protein amounts. For example, certain genes, such as *Igfbp3* and *Tnc* (displayed in blue) as well as *Ckb* and *Eef1a1* (displayed in red) showed respectively higher or lower than expected mRNA transcript levels based on emPAI values while several others, such as *Ecgr4*, *H1-2*, *H4c1*, and *H2ac4*, were not detected at all on a transcript level (Fig. 3D).

2.4. Comparison of RNAseq transcripts in cultured versus freshly isolated NSPCs reveals strong overall correlation between in vitro and in vivo NSPCs

To explore how in vitro culturing might impact the NSPC secretome, we next compared our in vitro NSPC scRNAseq data with two previously published scRNAseq studies of in vivo adult hippocampal NSPCs (Shin et al., 2015; Hochgerner et al., 2018). In Hochgerner et al. (Hoch.), adult mouse dentate gyri were microdissected and dissociated into a single cell suspension for 10X Chromium sequencing followed by unbiased clustering analysis to assign individual cells to a cell phenotype cluster. In Shin et al., the authors dissected the dentate gyri of nestin-GFP transgenic mice and created a single cell suspension from which they manually selected GFP^+ cells for sequencing on an Illumina HiSeq platform. Transcriptome data was then used to arrange cells according to pseudotime reflecting differentiation from a quiescent RGL to an activated RGL and then to an early IPC. For comparison across datasets, Hoch single cell data from radial glial like cells (Hoch. RGLs, which correspond to qRGL-NSCs), neural intermediate precursor cells (Hoch. nIPCs which correspond to aRGL-NSCs), and neuroblasts (Hoch. IPC/NBs, which correspond to a mixture of IPCs and NBs), were combined to generate an average transcript count for each cell population. The transcript counts from Shin data were averaged between pseudotime points 0 and 0.479 to form the Shin qRGL group and between pseudotime points 0.506 and 1 to form the Shin aRGL group.

Pearson correlation analysis was performed with all transcripts that were detected above 0 in all scRNAseq datasets. All correlations between compared populations were significant, though they varied in strength. Within the scRNAseq dataset from cultured NSPCs, near perfect correlation between clusters 0-5 was observed, with Pearson r values ranging from 0.97 to 0.99 (Fig. 4B). Comparison of in vitro NSPC subpopulations with in vivo qRGLs revealed overall higher correlations with the Shin qRGLs (r values ranging 0.39 to 0.42) than with the Hochgerner qRGLs (r values ranging from 0.29 to 0.31), and the strongest in vitro versus in vivo correlation was between Shin qRGLs and in vitro cluster 0 ($r(12504) = 0.42$, $p < 0.0001$), which we previously identified as qRGLs by expression of known qRGL markers (Fig. 1C and Supplemental Fig. 1E). Whether the differences in correlation strength of gene expression between in vitro NSPCs and qRGLs

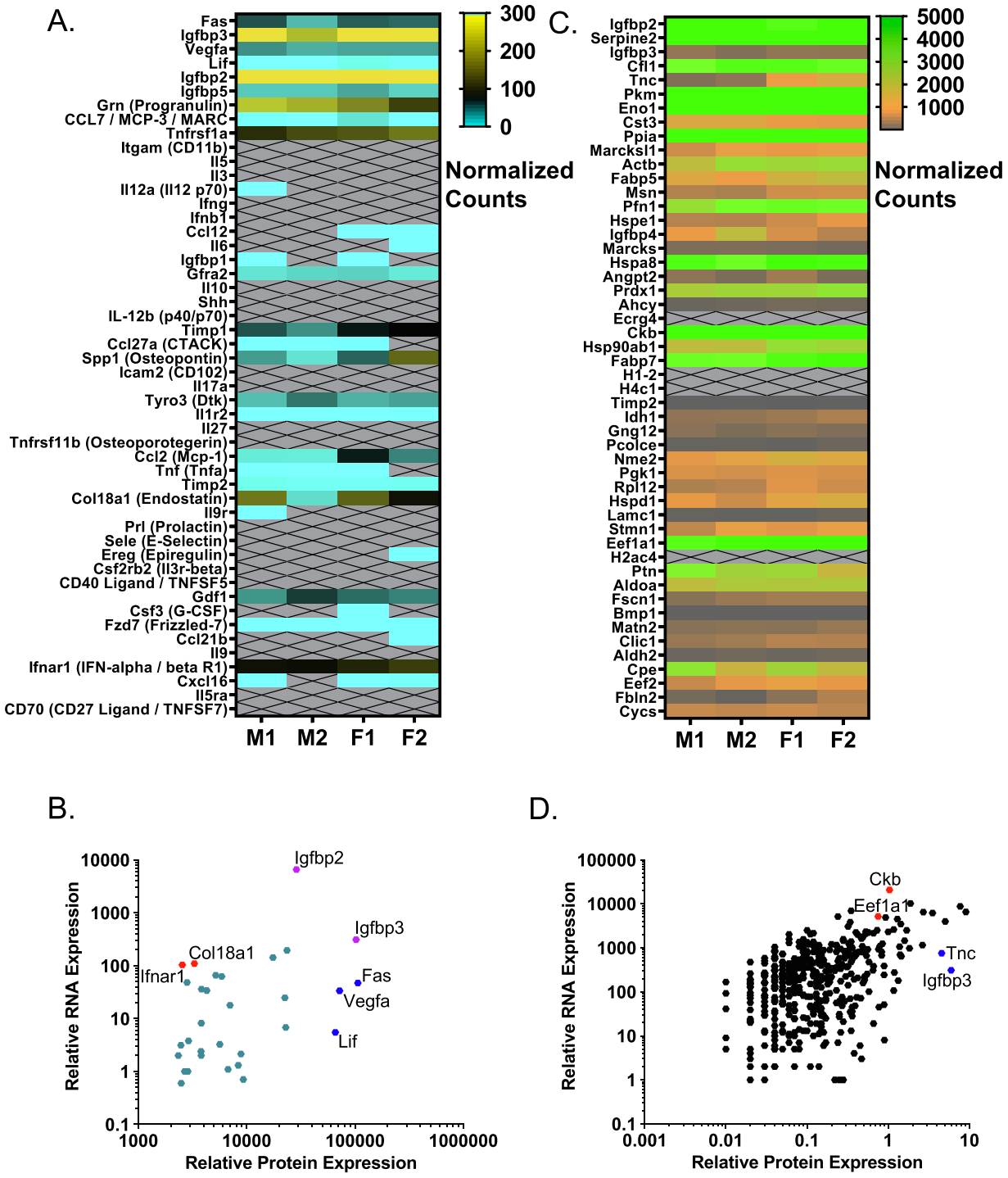

Fig. 3. Comparison of protein abundance and relative transcript levels for in vitro NSPCs. (A) Heatmap of in vitro transcript level expression in bulk RNAseq of top 50 secreted factors identified in protein array. (B) Scatter plot of relative transcript expression in bulk RNAseq to relative protein abundance in the protein array for the top 50 array factors. Z-score of fluorescence normalized to average fluorescence intensity within each slide used as relative protein expression values. (C) Heatmap of transcript expression for top 50 secreted proteins identified by LC-MS/MS of BONCAT-enriched NSPC CM-derived proteins. (D) Scatter plot of relative transcript expression in bulk RNAseq to relative protein abundance in LC-MS/MS of NSPC CM. All RNA expression values are gene length normalized counts. (M = male, F = female).

from the two in vivo datasets reflect differences in the cells profiled (different mouse strains, housing conditions) or technical artefact of different scRNAseq platforms is unclear. In contrast to qRGLs, aRGLs showed comparable, strong correlations between in vitro NPSCs and both Shin and Hochgerner aRGLs, as well as Hochgerner IPC/NBs (r ranging from 0.54 to 0.56). Notably, correlations between parallel in vivo RGL populations were 0.44 (qRGL) and 0.53 (aRGL), a similar strength as correlations between in vivo and in vitro populations in most cases. These data suggest that measured transcriptomic differences between in vitro NSPCs and in vivo counterparts does not greatly exceed measured differences between two separate analyses of in vivo cells and therefore that culture of these cells did not grossly alter the NSPC transcriptome in ways detectable by RNAseq.

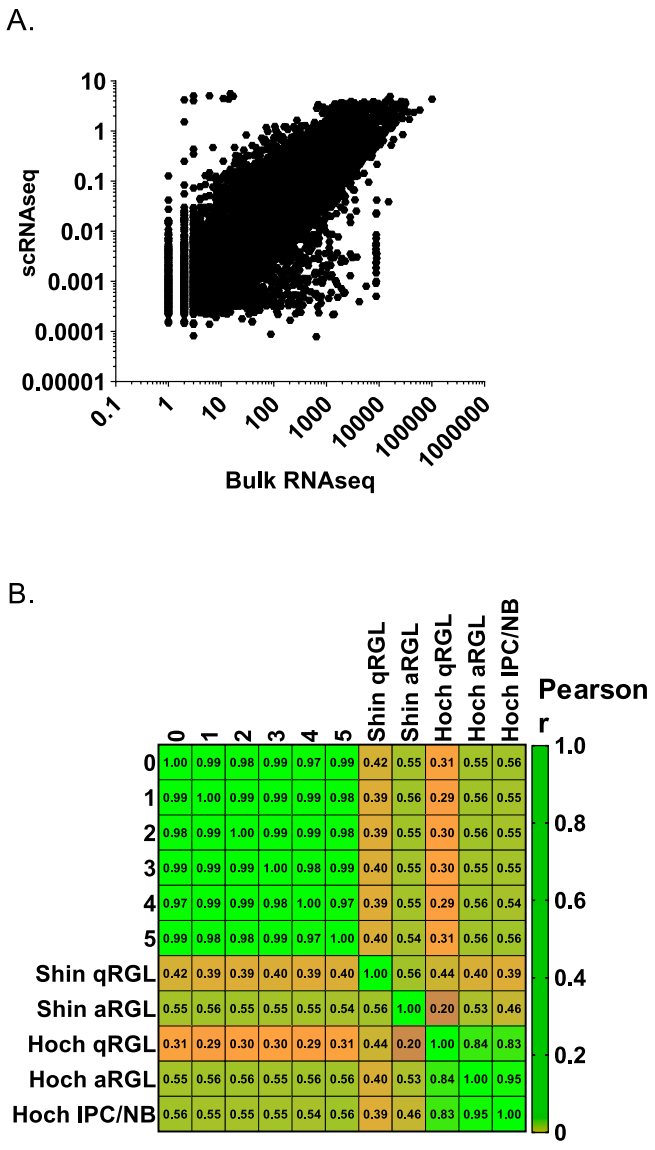

Fig. 4. Comparison of in vivo versus in vitro transcriptomes. (A) Scatter plot of relative transcript expression in bulk RNAseq versus scRNAseq of cultured NSPCs. (B) Matrix plot of relative transcript expression in in vitro NSPC clusters versus in vivo Shin qRGL, Shin aRGL, Hoch. qRGL, Hoch. aRGL, and Hoch. IPCs/NB groups. R values are displayed inside individual cells. All RNA expression represented as averaged counts for all cells within the population.

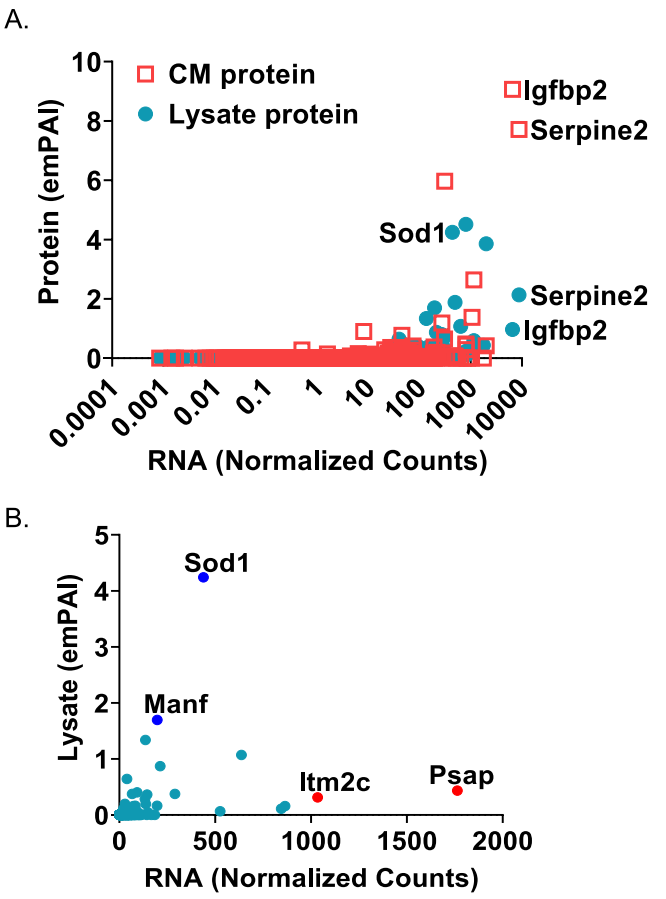

Fig. 5. Correlation of transcript level with protein abundance for GO term identified extracellular proteins from bulk RNAseq of cultured NSPCs. (A) Scatter plot of relative protein abundance determined by LC-MS/MS of BONCAT-enriched NSPC CM-derived proteins and of lysate-derived proteins relative to transcript expression for genes encoding extracellular proteins. (B) Scatter plot of relative protein abundance determined by LC-MS/MS of cultured NSPC lysate relative to transcript expression for genes encoding extracellular proteins that are not detected in NSPC CM. All RNA expression values are gene length normalized counts.

2.5. The NSPC transcriptome frequently fails to accurately predict the NSPC secretome

To determine the utility of RNAseq in predicting the NSPC secretome, we performed Gene Ontology (GO) analysis of all transcripts detected above zero in the bulk RNAseq of in vitro NSPCs and identified over 600 genes with transcript levels greater than zero that encode proteins located in the extracellular region (Supplemental Table 6). Of these genes, 72 were detected above zero at the protein level in LC-MS/MS of in vitro NSPC CM and 55 were found in LC-MS/MS of in vitro NSPC lysate (Supplemental Table 6). Comparison of relative RNA transcript levels with relative protein levels showed that, in general, genes with higher transcript counts were more likely to show higher protein abundance in both the lysate ($r(8\ 8\ 7) = 0.3975$, $p < 0.0001$) and CM ($r(8\ 8\ 7) = 0.3881$, $p < 0.0001$) (Fig. 5A). However, there were numerous genes with high transcriptional expression, but little to no protein level expression in CM or lysate. This discrepancy may be related to the phenomenon of "lineage priming" observed in SVZ NSCs where neurogenic and neuronal gene transcripts are abundantly transcribed, but are not translated (Baser et al., 2019; Kjell et al., 2020; Beckervordersandforth et al., 2010; Lepko et al., 2019). If RNA expression were being used to predict the secretome, these genes would represent a group that would be falsely identified as major components of the NSPC secretome. Focusing on proteins that were not present in CM revealed several proteins with high transcript and intracellular protein levels (*Manf* and *Sod1*, displayed in blue), suggesting high protein production but absence of secretion (Fig. 5B). However, SOD1 is also a protein exogenously provided in NSPC growth media and the high internal protein levels despite low transcript levels may also indicate potential internalization of SOD1 from the media. In addition, several proteins were also found that had high gene expression but low intracellular protein levels (e.g. *Itm2c* and Psap, displayed in red), suggesting low translation of these transcripts (Fig. 5B). All together, these data suggest that using RNA expression from high throughput techniques like RNAseq to prospectively identify major components of the secretome may lead to false positives due to translational and secretion-level regulation.

3. Discussion

Over the past decade, stem cell secretomes have been investigated

for their potential therapeutic applications to various neurologic disorders (Drago et al., 2013; Baraniak and McDevitt, 2010; Liang et al., 2014). The cytokines, chemokines, and growth factors that comprise the NSPC secretome have been thus far identified individually or in limited combinations with traditional methods of protein analysis such as immunohistochemistry, western blotting, and ELISA (Skalnikova et al., 2011). In other tissue stem cells, broader characterization of secreted proteins has been achieved with array based methods examining isolated stem cell populations maintained in vitro (Skalnikova et al., 2011). More recently, in vivo stem cell profiling with low cell and scRNAseq has emerged as a proxy for untargeted protein level analysis in small populations like NPSCs that do not yield sufficient protein for high-throughput translational-level analysis (Artegiani et al., 2017; Hochgerner et al., 2018; Shin et al., 2015). Cumulatively, these methods have provided several informative pieces of the puzzle. Our findings at the transcriptional level as well as the protein level in vitro provide a first attempt at a comprehensive analysis of the NSPC secretome, and, in the process, highlight limitations to current approaches.

Using a commercially-available array of over 300 preselected antibodies, we probed the CM of cultured NSPCs to generate a list of highly secreted factors, as is common for studies of secretome profiling (Skalnikova et al., 2011). Unexpectedly, though, further scrutiny of selected "top" targets by ELISA and an unbiased screen for secreted factors via LC-MS/MS based approaches revealed minimal corroboration of the array results. For example, quantification by ELISA of VEGFA and IGFBP-2 revealed over 10 fold more IGFBP-2 than VEGFA in contrast to the array fluorescence signal which ranked VEGFA slightly higher than IGFBP-2. LC-MS/MS analysis of cell lysate and CM confirmed the ELISA results, showing high levels of IGFBP-2 while VEGFA did not reach the detection limit of this method. More broadly, while most of the top 50 proteins by array were not detected by LC-MS/MS, proteins from near the bottom of the array ranking, such as Fractalkine (X3CL1), VEGFC, and MFGE8, were detected by LC–MS/MS. These data suggest that the fluorescence intensity values of the array used in the present work do not accurately represent relative protein abundance.

Ideally, factors identified in an antibody-based screen would undergo additional validation with methods including ELISA or LC-MS/MS as presented here. However, while ELISA and LC-MS/MS-based methods for protein quantification likely provide more accurate protein identification and quantification, they also have limitations.

First, LC-MS/MS has a relatively high minimum threshold required for protein detection. The provision of exogenous proteins in cell culture media, even when these proteins are known, can reduce sensitivity for identifying cell-derived proteins. We used recently-developed protocols for enriching the cell-derived secretome via BONCAT (Mahdavi et al., 2016; Liu et al., 2017; Elliott et al., 2014) to boost sensitivity without supplement-depriving cultured NSPCs. BONCAT has been previously shown to not alter the proteome or secretome in detectable ways (Mahdavi et al., 2016; Liu et al., 2017; Dieterich et al., 2006) and we also confirmed that cultured NSPCs showed no overt signs of proteomic changes due to incorporation of non-canonical amino acids in the nascent proteins. However, it is still possible that BONCAT alters the proteome of NSPCs and this possibility should be considered when evaluating data from BONCAT-enriched proteomes. In addition, even with BONCAT enrichment, LC-MS/MS showed somewhat low sensitivity. For example, VEGFA was readily detected in CM and cell lysate by ELISA, but it was not detected in BONCAT enriched LC-MS/MS of CM. Meeting the threshold level of detection for LC-MS/MS likely excluded detection of other NSPC-produced factors that may have biologically relevant functions.

In contrast to LC–MS/MS, ELISAs are frequently capable of detecting picogram amounts of protein in CM. However, they are only able to assess one protein at a time. Verifying a broad secretome screen via ELISA may frequently be impractical due to the time and cost of numerous ELISAs. Additionally, given how few of the top array factors were confirmed by LC-MS/MS, our data seems to suggest that pursuing numerous validations of top array factors by ELISA may not be advisable. These respective limitations should be considered when choosing a method for proteomic profiling of the secretome and interpreting its results.

We also examined the NSPC secretome at the transcriptional level via RNAseq. Bulk and single cell RNAseq data confirmed the identity of NSPC cultures as primarily quiescent and activated NSCs in various stages of the cell cycle. Overall correlation between gene-length normalized mRNA transcript counts of cultured NSPCs and relative protein abundance in cultured NSPC CM by LC-MS/MS was only moderate (Fig. 3D), suggesting that transcriptional expression is not a direct measure of secreted protein abundance. Furthermore, attempting to prospectively predict highly secreted proteins from the transcriptional expression of genes coding for extracellularly located proteins was less reliable. Here, we found a subpopulation of factors that were high in mRNA abundance, but low in abundance or completely absent from NSPC CM at the protein level. This finding may be related to the phenomenon of neuronal "linage priming" that has been noted in NSCs in the SVZ neurogenic niche (Baser et al, 2019; Beckervordersandforth et al., 2010; Kjell et al., 2020; Lepko et al., 2019). In "linage priming", certain genes that regulate neuronal differentiation are highly transcribed and poised for translation once differentiation is officially initiated, allowing for lineage amplification. These genes appeared to be regulated at the translational level as their protein amounts were low in cell lysate despite high transcript levels. Several other genes appeared to be regulated at the secretion level as their protein abundance intracellularly was high despite begin being absent from CM. These disparities emphasize the importance of involving protein-level analyses to transcript-level analyses when identifying secretome components and suggest a potential pitfall of defining a secretome based on transcriptional data.

Significant changes to cell physiology secondary to culturing have been reported for other stem cell populations (Binato et al., 2013; Duggal et al., 2009; Duggal and Brinchmann, 2011; Wernly et al., 2017; Shahdadfar et al., 2005). In fact, cultured NSCs isolated from the SVZ displayed important differences in transcription of inflammatory cytokines compared to their in vivo counterparts (Dulken et al., 2017). Comparison of the present in vitro scRNAseq dataset with two previously published in vivo DG NSPC scRNAseq datasets showed moderate to strong correlations in gene expression (Shin et al., 2015; Hochgerner et al., 2018). These correlations suggest overall global agreement in relative transcriptional profiles, and support the utility of adult DG NSPC cultures as a model of their in vivo counterpart. However, future analyses of specific gene expression patterns between these datasets are required to determine whether the differences that do exist between datasets reflect true differences in cell physiology. Study of both cultured and acutely isolated stem cells is particularly critical for the development of effective NSPC-based therapies as current clinical trials use cultured neural stem cell lines and many preclinical models use NSPCs with varying amounts of in vitro processing (Mazzini et al., 2019; Ottoboni et al., 2017; Mendes-Pinheiro et al., 2018; Chandanala et al., 2014).

In conclusion, we provide a multi-level characterization of the NSPC secretome, in the process, identifying potentially important differences between protein and RNA expression in NSPCs and highlighting limitations in current methods of secretome profiling. Combined, our data suggest that no one method or level of analysis is sufficient for characterizing the NSPC secretome and we propose that the various proteins identified here as highly expressed in different platforms represent a putative NSPC secretome that requires subsequent validation. As stem cell-based therapies are currently being developed with both cultured and endogenous cells, our findings suggest that the optimal approach is a multifaceted one that includes unbiased global proteome analysis in conjunction with transcriptome analysis for the comprehensive characterization of in vitro and in vivo NSPCs.

4. Experimental procedures

4.1. Animals

Male and female C57BL/J6 mice (Jackson, stock #000664) aged 8–10 weeks were group housed (up to 5 per cage) in standard ventilated cages with food and water ad libitum on a 12 h light cycle. Animals were anesthetized with intraperitoneal injections of 87.5 mg/kg ketamine/12.5 mg/kg xylazine before perfusion and harvest of brains for primary cell derivations. This study was approved by the Institutional Animal Care and Use Committee (IACUC) at the Ohio State University.

4.2. Cell culture

NSPCs were isolated from adult DGs of C57BL/6J mice as described in (Babu et al., 2011). NSPCs were cultured on poly-D-lysine (Sigma) and laminin (Invitrogen) coated plates in Neurobasal A media (Invitrogen) with 1x B27 supplement without vitamin A (Gibco), 1x glutamax (Invitrogen) and 20 ng/ml each of EGF and FGF2 (Peprotech). All cells used were between passage five and 15. Two separate lines were used in experiments, one from 4 pooled C57BL/6J male mice and one from 4 pooled C57BL/6J female mice. No inherent differences in morphology or proliferation between NSPCs isolated from males and females were found. Both lines were verified to be mycoplasma-free and to produce neurons and glia upon culture in differentiation conditions. NSPCs were differentiated according to the growth factor withdrawal protocol described in Babu et al. (2011).

4.3. Immunofluorescence

NSPCs were cultured in chamber slides under maintenance or differentiation conditions described above. Cells were fixed with 4% paraformaldehyde (PFA) then rinsed in 1× phosphate buffered saline (PBS) before blocking with 1% normal donkey serum (Jackson) and 0.3% Triton X-100 in PBS for 1 h at room temperature. Cells were incubated with primary antibodies (Supplemental Table 7) overnight at 4 °C in blocking solution on an orbital shaker. The next day, cells were washed with PBS and incubated with fluorescently conjugated secondary antibodies diluted in blocking solution (Supplemental Table 7) for 2 h at room temperature. 10 min incubation with Hoechst 33342 (Fisher, 1:2000) was then used to label DNA in nuclei. After washing, chambers were removed from slides and cells were coverslipped with ProLong Gold anti-fade solution (Molecular Probes) before imaging on a Zeiss Axio Observer Z.1 with apotome digital imaging system and Axiocam 506 monochrome camera (Zeiss).

For BONCAT optimization studies, NSPCs were cultured in 96 well plates. At 80% confluence, NSPC growth media was replaced with methionine-depleted neurobasal A (Gibco) containing 1× B27 supplement without vitamin A (Gibco), 1× glutamax (Invitrogen), 20 ng/ml each of EGF and FGF2 (Peprotech) for 30 min. After 30 min of methionine washout, growth media containing 12.5 μM methionine (Gibco), 1x B27 supplement without vitamin A (Gibco), 1x glutamax (Invitrogen), 20 ng/ml each of EGF and FGF2 (Peprotech) and 100 μM AHA (Click Chemistry Tools) or water vehicle was added to NSPCs which were incubated for 24 h at 37 °C and 5% CO_2. After 24 h, 20 μM BrdU was added to cells for 2 h prior to fixation. Cells were stained in 96 well format for BrdU and Hoechst 33342 or DBCO IR800 (Supplemental Table 7).

For BrdU, cells were fixed with 4% PFA for 10 min and blocked with 1% normal donkey serum (Jackson) and 0.3% Triton X-100 in PBS for 1 h at room temperature before a 30 min antigen retrieval with 2 N hydrochloric acid a 37 °C. Cells were then incubated with anti-BrdU antibody overnight at 4 °C. After 3 washes with PBS, cells were incubated with secondary antibody for 2 h at room temperature, protected from light. Hoechst 33342 was added for the last 10 min of secondary antibody incubation. Cells were washed three times with PBS before imaging on the Zeiss Axio Observer Z.1.

For DBCO IR800, AHA-treated NSPCs were fixed with ice cold methanol and washed with PBS three times before treatment with iodoacetamide for 90 min at room temperature, protected from light.12 μM DBCO IR800 was spiked in to the wells and the plate was incubated at room temperature for 30 min, protected from light. Cells were washed with PBS three times before aspirating all buffer and imaging the plate on LICOR Odyssey.

4.4. Cytokine antibody array

Conditioned media was generated from three separate cultures of NSPCs, one male and two female, at 80% confluence. After 48 h of culture, media was collected and centrifuged at 1000*g* for 10 min to remove large debris. For sample normalization, NSPCs for each corresponding conditioned media sample were also harvested with accutase (Invitrogen) and total protein was quantified with a BCA protein assay kit (Pierce) per manufacturer recommendations. Preparation and staining of slides were completed per manufacturer recommendations with the following modifications (RayBiotech L308 cytokine antibody array). The second dialysis step both before and after labeling of samples with biotin were conducted overnight at 4 °C. Incubation of slides with biotin-labeled samples was also conducted overnight at 4 °C. Incubation with Cy3-conjugated streptavidin was conducted for two hours at room temperature. After completion of the protocol, slides were completely dried before they were stored at −20 °C in the 30 mL centrifuge tube provided by the manufacturer until processing. Slides were scanned by RayBiotech and raw data was analyzed according to manufacturer instructions using the RayBio Analysis Tool Software.

4.5. ELISA

Conditioned media was generated after a 24 h incubation of complete growth media with NSPCs between passages 5 and 15 at 80% confluence. After collection of media, cells were then lysed with RIPA buffer (Thermo) containing Halt protease inhibitor cocktail (Thermo) and cell lysate was stored at −20 °C. Conditioned media samples were centrifuged to remove debris as above, aliquoted, and stored at −20 °C until use. VEGF, IGFBP-2, LIF, and FASL ELISAs (all R&D Systems) were performed per manufacturer instructions. All standards were created in NSPC growth media for conditioned media samples and RIPA buffer for cell lysates. Microplates were read with an Epoch microplate reader (Biotek) at 450 nm wavelength.

4.6. Mass spectrometry

For LC–MS/MS of NSPC cell lysate, NSPCs were harvested with accutase (Invitrogen) and washed with Hank's balanced salt solution (HBSS) before processing by the Ohio State University CCIC Mass Spectrometry and Proteomics Facility as described below.

LC–MS/MS of NSPC BONCAT enriched conditioned media-derived proteins was performed according to a modification of the protocol of Dieterich et al. (2006). CM containing AHA-tagged proteins was generated with male and female NSPCs between passage five and 15. At 80% confluence, NSPCs in 10 cm dishes between passage 5 and 15 were methionine depleted for 30 min by incubation with neurobasal A without methionine (Gibco), 1× B27 supplement without vitamin A (Gibco), 1× glutamax (Invitrogen) and 20 ng/ml each of EGF and FGF2 (Peprotech). After 30 min, media was replaced with 5 mL neurobasal A containing 12.5 μM methionine (Gibco), 1× B27 supplement without vitamin A (Gibco), 1× glutamax (Invitrogen), 20 ng/ml each of EGF and FGF2 (Peprotech) and 100 μM AHA (Click Chemistry Tools) or water vehicle. After 24 h, conditioned media was collected and centrifuged at 1000*g* for 10 min to remove large debris. Conditioned media was then concentrated with 3 kDa Amicon Ultra filters according to manufacturer instructions (Millipore) to ~250 μl total volume. PBS was

then added to the remaining concentrate up to the maximum capacity of the filter unit to dilute free AHA followed by a second round of concentration. The final concentrate was mixed with an equal volume of water with protease inhibitors (Roche) and sonicated five times with one second pulses at 50% amplitude (Fisher). Samples were contrifuged at 15,000*g* for 5 min and supernatants were treated with 50 μM iodoacetamide (Pierce) for 90 min in the dark. 100 μl of DBCO magnetic beads per sample were washed with 100 μl PBS 3 times before being resuspended in iodoacetamide-treated conditioned media concentrates. Beads were rotated end-over-end for 16–18 hrs. Beads were then washed with 400 μl of 0.8% SDS in PBS 8 times, 400 μl of 8 M urea eight times, and 400 μl of 20% acetonitrile eight times before transfer to the Ohio State University CCIC Mass Spectrometry and Proteomics Facility.

In preparation for protein digest, beads were washed with 50 μl of 50 mM ammonium bicarbonate three times. Each time, the supernatants were kept and pooled. After the third wash, 5 μl of DTT (5 μg/μL in50 mM ammonium bicarbonate) was added and the samples were incubated at 56 °C for 15 min. After the incubation, 5uL of iodoacetamide (15 mg/ml in 50 mM ammonium bicarbonate) was added and the sample was kept in dark at room temperature for 30 min. Sequencing grade-modified trypsin (Promega, Madison WI) prepared in 50 mM ammonium bicarbonate was added to the sample with an estimation of 1:20 /1:100 enzyme-substrate ratio and the reaction was carried on at 37 °C for overnight. The reaction was quenched the next morning by adding acetic acid for acidification. Supernatant was then concentrated for LC-MS/MS analysis with the Thermo Scientific Orbitrap Fusion mass spectrometer equipped with an EASY-Spray Sources operated in positive ion mode. Samples (6.4 μl) were separated on an easy spray nano column (PepmapTM RSLC, C18 3μ 100A, 75 μm X150mm Thermo Scientific) using a 2D RSLC HPLC system from Thermo Scientific. Each sample was injected into the μ-Precolumn Cartridge (Thermo Scientific) and desalted with 0.1% formic acid in water for 5 min. The injector port was then switched to inject and the peptides were eluted off of the trap onto the column. Mobile phase A was 0.1% formic acid in water and acetonitrile (with 0.1% formic acid) was used as mobile phase B. Flow rate was set at 300 nL/min. A 2 h gradient was used: mobile phase B was increased from 2% to 20% in 105 min and then increased from 20 to 32% in 10 min and again from 32 to 95% in 1 min and then kept at 95% for another 4 min before being brought back quickly to 2% in 1 min. The column was equilibrated at 2% of mobile phase B (or 98% A) for 15 min before the next sample injection.

LC-MS/MS data was acquired with a spray voltage of 1.6 KV and a capillary temperature of 305 °C is used. The scan sequence of the mass spectrometer was based on the preview mode data dependent TopSpeed™ method: the analysis was programmed for a full scan recorded between m/z 375–1500 and a MS/MS scan to generate product ion spectra to determine amino acid sequence in consecutive scans starting from the most abundant peaks in the spectrum in the next 3 s. To achieve high mass accuracy MS determination, the full scan was performed at FT mode and the resolution was set at 120,000 with internal mass calibration. The AGC Target ion number for FT full scan was set at 4 × 105 ions, maximum ion injection time was set at 50 ms and micro scan number was set at 1. MSn was performed using HCD in ion trap mode to ensure the highest signal intensity of MSn spectra. The HCD collision energy was set at 32%. The AGC Target ion number for ion trap MSn scan was set at 3.0E4 ions, maximum ion injection time was set at 35 ms and micro scan number was set at 1. Dynamic exclusion is enabled with a repeat count of 1 within 60 s and a low mass width and high mass width of 10 ppm.

Sequence information from the LC-MS/MS data was processed by converting the .raw files into a merged file (.mgf) using MSConvert (ProteoWizard). The resulting mgf files were searched against the most recent Uniprot databases using Mascot Daemon by Matrix Science version 2.5.1 (Boston, MA). A decoy database was also searched to determine the false discovery rate (FDR) and peptides were filtered according at 1% FDR. Proteins identified with at least two unique peptides were considered as reliable identification. Any modified peptides are manually checked for validation.

4.7. Bulk RNAseq RNA isolation, cDNA library construction, and sequencing

Approximately 30,000 cells from two female and two male adult NSPCs cultures were harvested with accutase (Stem Cell Technologies) and washed with PBS before RNA isolation with the Clontech Nucleospin RNA XS Plus isolation kit (Takara 740990.10) per manufacturer protocol. RNA was also isolated from whole DGs isolated from one male and one female C57/Bl6 mouse with the same kit. RNA quality and quantity was assessed with a Qubit RNA HS assay kit (Invitrogen). All cultured samples used had a RIN value of 10 while whole DG samples had RIN values over 8. Libraries were generated with the NEBNext Ultra II Directional RNA Library prep kit (New England Biolabs) for the whole DGs and the Clontech SMART-Seq HT (Takara) kit for cultured NSPCs. Purified library products were then used in HiSeq 4000 paired-end sequencing (Illumina) to a depth of 15–20 million 2 × 150 bp clusters.

4.8. Bulk RNAseq analysis

Individual FASTQ files were trimmed for adapter sequences and filtered for a minimum quality score of Q20 using AdapterRemoval v2.2.0. Preliminary alignment using HISAT2 v2.0.6 was performed to a composite reference of rRNA, mtDNA, and PhiX bacteriophage sequences obtained from NCBI RefSeq. Reads aligning to these references were excluded in downstream analyses. Primary alignment was performed against the mouse genome reference GRCm38p4 using HISAT2. Gene expression values for genes described by the GENCODE Gene Transfer Format (GTF) release M14 (mouse) were quantified using the featureCounts tool of the Subread package v1.5.1 58 in stranded mode.

4.9. scRNA sequencing and analysis

One male and two female NSPCs between passage 7 and 12 were harvested from adherent culture. Cells were resuspended and washed in HBSS before making a mixed sample with equal numbers from each NSPC culture for scRNAseq. 10× Genomics 3′ RNA-seq library was sequenced using paired-end 150 bp approach on an Illumina HiSeq 4000 sequencer. CellRanger v3.1.0 (Zheng et al., 2017) was used to demultiplex, align, and deduplicate sequencing reads in BCL files. Single-cell data in feature-barcode matrices were then processed using Seurat v3.1.0's default pipeline (Butler et al., 2018) to identify unsupervised cell clusters and generate a t-Distributed Stochastic Neighbor Embedding (t-SNE) plot. Seurat's feature expression analysis was used to visualize genes markers known to be expressed in cell populations displayed in the t-SNE plot.

4.10. Quantitative rt-PCR

For qrt-PCR, all RNA was isolated and DNase treated with the BioRad Aurum™ Total RNA Mini Kit. In vitro NSPCs were lysed in culture plates and then transferred to spin columns provided by the BioRad Aurum™ kit. For the positive controls, a spleen was extracted from an adult C57BL/6J mouse and minced before lysis with lysis buffer from the Bio Rad Aurum™ kit. Isolated RNA was quantified and assessed for quality using the BioTek Epoch Microplate Spectrophotometer. cDNA was synthesized with the BioRad iScript™ cDNA Synthesis Kit in the ThermoFisher Applied Biosystems 2720 Thermal Cycler. qrtPCR was performed in the Bio Rad CFX96 Touch Real-Time PCR Detection System with BioRad SsoAdvanced Universal SYBR Green Supermix and primers listed in Supplemental Table 7. Ct values were determined from raw amplification data using Real-time PCR Miner software (Zhao and Fernald, 2005). The PCR Miner Ct output was converted to fold change

relative to the Ct value for the housekeeping gene *sdha*.

4.11. Statistics

Fluorescence intensity for each protein in the protein array was normalized to the average fluorescence intensity within each slide. Z-scores were calculated in Microsoft Excel and a heatmap of top 50 secreted factors was generated with Prism Graphpad software. For Spearman correlation with RNAseq data, fluorescence values normalized to the average fluorescence intensity within each slide were calculated in Microsoft Excel before statistical analysis and graphical representation with Prism Graphpad software.

For all ELISAs, absolute protein concentrations for each sample were determined based on the standard curve and graphically represented using Prism Graphpad software.

For RNAseq analysis, published data was retrieved in Excel format from (Shin et al., 2015) and (Hochgerner et al., 2018). scRNAseq counts for each gene were averaged to generate a representative count for each population. Shin qRGLs were averaged from pseudotime point 0 to 0.479. Shin aRGLs were averaged from pseudotime point 0.506 to 1. Pearson correlations were completed between the cultured NSPC clusters, Shin qRGL, Shin aRGL, Hoch. qRGL, Hoch aRGL, and Hoch IPC/NB scRNAseq counts averaged over cell type for each population. All correlation statistics ($\alpha = 0.05$) were completed for gene length normalized counts for bulk RNAseq, emPAI values for LC-MS/MS data, or averaged counts for scRNAseq with Prism Graphpad software.

4.12. Data availability

Processed reads for NSPC bulk RNAseq data are provided as Supplemental Table 1. Processed reads for NSPC scRNAseq are provided for each cell by cluster in Supplemental Tables 8-13. Raw data files for both the bulk RNAseq and scRNAseq datasets are publicly available in GEO (GSE138381).

Declaration of Competing Interest

The authors declare that they have no known competing financial interests or personal relationships that could have appeared to influence the work reported in this paper.

Acknowledgements

This work was supported by R00NS089938 to EDK from the NIH/NINDS, and IOS-1923094 to EDK from NSF. The Fusion Orbitrap instrument was supported by NIH Award Number Grant S10 OD018056.

Appendix A. Supplementary data

Supplementary data to this article can be found online at https://doi.org/10.1016/j.brainres.2020.146717.

References

Alvarez-Castelao, Beatriz, Schanzenbächer, Christoph T., Langer, Julian D., Schuman, Erin M., 2019. Cell-type-specific metabolic labeling, detection and identification of nascent proteomes in vivo. Nat. Protoc. 14 (2), 556–575. https://doi.org/10.1038/s41596-018-0106-6.

Andres, Robert H., Horie, Nobutaka, Slikker, William, Keren-Gill, Hadar, Zhan, Ke, Sun, Guohua, Manley, Nathan C., et al., 2011. Human neural stem cells enhance structural plasticity and axonal transport in the ischaemic brain. Brain 134 (6), 1777–1789. https://doi.org/10.1093/brain/awr094.

Artegiani, Benedetta, Lyubimova, Anna, Muraro, Mauro, van Es, Johan H., van Oudenaarden, Alexander, Clevers, Hans, 2017. A single-cell RNA sequencing study reveals cellular and molecular dynamics of the hippocampal neurogenic niche. Cell Rep. 21 (11), 3271–3284. https://doi.org/10.1016/j.celrep.2017.11.050.

Babu, Harish, Claasen, Jan-Hendrik, Kannan, Suresh, Rünker, Annette E, Palmer, Theo, Kempermann, Gerd, 2011. A protocol for isolation and enriched monolayer cultivation of neural precursor cells from mouse dentate gyrus. Front. Neurosci. 5, 89. https://doi.org/10.3389/fnins.2011.00089.

Bacigaluppi, Marco, Sferruzza, Giacomo, Butti, Erica, Ottoboni, Linda, Martino, Gianvito, 2020. Endogenous neural precursor cells in health and disease. Brain Res. 1730 (March), 146619. https://doi.org/10.1016/J.BRAINRES.2019.146619.

Baraniak, Priya R., McDevitt, Todd C., 2010. Stem cell paracrine actions and tissue regeneration. Regenerative Med. 5 (1), 121–143. https://doi.org/10.2217/rme.09.74.

Barkho, Basam Z, Song, Hongjun, Aimone, James B, Smrt, Richard D, Kuwabara, Tomoko, Nakashima, Kinichi, Gage, Fred H, Zhao, Xinyu, 2006. Identification of astrocyte-expressed factors that modulate neural stem/progenitor cell differentiation. Stem Cells Dev. 15 (3), 407–421. https://doi.org/10.1089/scd.2006.15.407.

Baser, A., et al., 2019. Onset of differentiation is post-transcriptionally controlled in adult neural stem cells. Nature 566, 100–104.

Beckervordersandforth, et al., 2010. In vivo fate mapping and expression analysis reveals molecular hallmarks of prospectively isolated adult neural stem cells. Cell Stem Cell 7, 744–758.

Besse, Florence, Ephrussi, Anne, 2008. Translational control of localized MRNAs: restricting protein synthesis in space and time. In: Nat. Rev. Mol. Cell Bio. Nature Publishing Group. https://doi.org/10.1038/nrm2548.

Binato, R., de Souza Fernandez, T., Lazzarotto-Silva, C., Du Rocher, B., Mencalha, A., Pizzatti, L., Bouzas, L.F., Abdelhay, E., 2013. Stability of human mesenchymal stem cells during *in Vitro* Culture: considerations for cell therapy. Cell Prolif. 46 (1), 10–22. https://doi.org/10.1111/cpr.12002.

Butler, Andrew, Hoffman, Paul, Smibert, Peter, Papalexi, Efthymia, Satija, Rahul, 2018. Integrating single-cell transcriptomic data across different conditions, technologies, and species. Nat. Biotechnol. https://doi.org/10.1038/nbt.4096.

Chandanala, Shashank, Ys, Harishchandra Prasad, Venugopal, Chiatra, Dhanushkodi, Anandh, 2014. Stem cells based therapy for temporal lobe epilepsy. J. Clin. Biomed. Sci. 4. www.jcbsonline.ac.in.

Dieterich, Daniela C., James Link, A., Graumann, Johannes, Tirrell, David A., Schuman, Erin M., 2006. Selective identification of newly synthesized proteins in mammalian cells using Bioorthogonal Noncanonical Amino Acid Tagging (BONCAT). PNAS 103 (25), 9482–9487. https://doi.org/10.1073/pnas.0601637103.

Drago, Denise, Cossetti, Chiara, Iraci, Nunzio, Gaude, Edoardo, Musco, Giovanna, Bachi, Angela, Pluchino, Stefano, 2013. The stem cell secretome and its role in brain repair. Biochimie 95 (12), 2271–2285. https://doi.org/10.1016/j.biochi.2013.06.020.

Duggal, Shivali, Brinchmann, Jan E., 2011. Importance of serum source for the in vitro replicative senescence of human bone marrow derived mesenchymal stem cells. J. Cell. Physiol. 226 (11), 2908–2915. https://doi.org/10.1002/jcp.22637.

Duggal, Shivali, Frønsdal, Katrine B., Szöke, Krisztina, Shahdadfar, Aboulghassem, Melvik, Jan Egil, Brinchmann, Jan E., 2009. Phenotype and gene expression of human mesenchymal stem cells in alginate scaffolds. Tissue Eng. Part A 15 (7), 1763–1773. https://doi.org/10.1089/ten.tea.2008.0306.

Dulken, Ben W., Leeman, Dena S., Boutet, Stéphane C., Hebestreit, Katja, Brunet, Anne, 2017. Single-cell transcriptomic analysis defines heterogeneity and transcriptional dynamics in the adult neural stem cell lineage. Cell Rep. 18 (3), 777–790. https://doi.org/10.1016/j.celrep.2016.12.060.

Durr, Eberhard, Jingyi, Yu., Krasinska, Karolina M., Carver, Lucy A., Yates, John R., Testa, Jacqueline E., Phil, Oh., Schnitzer, Jan E., 2004. Direct proteomic mapping of the lung microvascular endothelial cell surface in vivo and in cell culture. Nat. Biotechnol. 22 (8), 985–992. https://doi.org/10.1038/nbt993.

Elliott, Thomas S, Bianco, Ambra, Chin, Jason W, 2014. Genetic code expansion and bioorthogonal labelling enables cell specific proteomics in an animal. Curr. Opin. Chem. Biol. 21 (August), 154–160. https://doi.org/10.1016/j.cbpa.2014.07.001.

Gage, Fred H., Temple, Sally, 2013. Neural stem cells: generating and regenerating the brain. Neuron 80 (3), 588–601. https://doi.org/10.1016/j.neuron.2013.10.037.

Hochgerner, Hannah, Zeisel, Amit, Lönnerberg, Peter, Linnarsson, Sten, 2018. Conserved properties of dentate gyrus neurogenesis across postnatal development revealed by single-cell RNA sequencing. Nat. Neurosci. 21 (2), 290–299. https://doi.org/10.1038/s41593-017-0056-2.

Ishihama, Yasushi, Oda, Yoshiya, Tabata, Tsuyoshi, Sato, Toshitaka, Nagasu, Takeshi, Rappsilber, Juri, Mann, Matthias, 2005. Exponentially Modified Protein Abundance Index (EmPAI) for estimation of absolute protein amount in proteomics by the number of sequenced peptides per protein. Mol. Cell. Proteomics 4 (9), 1265–1272. https://doi.org/10.1074/mcp.M500061-MCP200.

Jewett, John C., Bertozzi, Carolyn R., 2010. Cu-free click cycloaddition reactions in chemical biology. Chem. Soc. Rev. 39 (4), 1272. https://doi.org/10.1039/b901970g.

Ji, Rui, Meng, Lingbin, Jiang, Xin, Cvm, Naresh Kumar, Ding, Jixiang, Li, Qiutang, Qingxian, Lu., 2014. TAM receptors support neural stem cell survival, proliferation and neuronal differentiation. PLoS One 9 (12), e115140. https://doi.org/10.1371/journal.pone.0115140.

Kalluri, Haviryaji S.G., Dempsey, Robert J., 2011. IGFBP-3 inhibits the proliferation of neural progenitor cells. Neurochem. Res. 36 (3), 406–411. https://doi.org/10.1007/s11064-010-0349-2.

Kirby, Elizabeth D., Kuwahara, Akela A., Messer, Reanna L., Wyss-Coray, Tony, 2015. Adult hippocampal neural stem and progenitor cells regulate the neurogenic niche by secreting VEGF. Proc. Natl. Acad. Sci. 112 (13), 4128–4133. https://doi.org/10.1073/pnas.1422448112.

Kjell, et al., 2020. Defining the adult neural stem cell niche proteome identifies key regulators of adult neurogenesis. Cell Stem Cell 26, 277–293. https://doi.org/10.1016/j.stem.2020.01.002.

Knight, Julia C, Scharf, Eugene L, Mao-Draayer, Yang, 2010. Fas activation increases neural progenitor cell survival. J. Neurosci. Res. 88 (4), 746–757. https://doi.org/10.1002/jnr.22253.

Lee, Eun Mi, Hurh, Sunghoon, Cho, Bumrae, Kook-Hwan, Oh., Kim, Seung U, Surh, Charles D, Sprent, Jonathan, Yang, Jaeseok, Kim, Jae Young, Ahn, Curie, 2013. CD70-CD27 ligation between neural stem cells and CD4+ T cells induces Fas-Fasl-

mediated T-cell death. Stem Cell Res. Ther. 4 (3), 56. https://doi.org/10.1186/scrt206.

Lepko, et al., 2019. Choroid plexus-derived miR-204 regulates the number of quiescent neural stem cells in the adult brain. EMBO 38.

Liang, Xiaoting, Ding, Yue, Zhang, Yuelin, Tse, Hung-Fat, Lian, Qizhou, 2014. Paracrine mechanisms of mesenchymal stem cell-based therapy: current status and perspectives. Cell Transplant. 23 (9), 1045–1059. https://doi.org/10.3727/096368913X667709.

Lipshitz, Howard D., Claycomb, Julie M., Smibert, Craig A., 2017. Post-transcriptional regulation of gene expression. Methods 126 (August), 1–2. https://doi.org/10.1016/J.YMETH.2017.08.007.

Liu, Yan, Conboy, Michael J., Mehdipour, Melod, Liu, Yutong, Tran, Thanhtra P., Blotnick, Aaron, Rajan, Prasanna, Santos, Thalie Cavalcante, Conboy, Irina M., 2017. Application of bio-orthogonal proteome labeling to cell transplantation and heterochronic parabiosis. Nat. Commun. 8 (1), 643. https://doi.org/10.1038/s41467-017-00698-y.

Mahdavi, Alborz, Hamblin, Graham D., Jindal, Granton A., Bagert, John D., Dong, Cathy, Sweredoski, Michael J., Hess, Sonja, Schuman, Erin M., Tirrell, David A., 2016. Engineered aminoacyl-TRNA synthetase for cell-selective analysis of mammalian protein synthesis. J. Am. Chem. Soc. 138 (13), 4278–4281. https://doi.org/10.1021/jacs.5b08980.

Mazzini, Letizia, Maurizio Gelati, Daniela Celeste Profico, Gianni Sorarù, Daniela Ferrari, Massimiliano Copetti, Gianmarco Muzi, et al. 2019. "Results from Phase I Clinical Trial with Intraspinal Injection of Neural Stem Cells in Amyotrophic Lateral Sclerosis: A Long-Term Outcome." STEM CELLS Translational Medicine 8(9): sctm.18-0154. DOI:10.1002/sctm.18-0154.

Mendes-Pinheiro, Bárbara, Teixeira, Fábio G., Anjo, Sandra I., Manadas, Bruno, Behie, Leo A., Salgado, António J., 2018. Secretome of undifferentiated neural progenitor cells induces histological and motor improvements in a rat model of parkinson's disease. Stem Cells Transl. Med. 7 (11), 829–838. https://doi.org/10.1002/sctm.18-0009.

Ming, Guo-li, Song, Hongjun, 2011. Adult neurogenesis in the mammalian brain: significant answers and significant questions. Neuron 70 (4), 687–702. https://doi.org/10.1016/j.neuron.2011.05.001.

Ottoboni, Linda, Merlini, Arianna, Martino, Gianvito, 2017. Neural stem cell plasticity: advantages in therapy for the injured central nervous system. Front. Cell Dev. Biol. 5 (May). https://doi.org/10.3389/fcell.2017.00052.

Ourednik, Jitka, Ourednik, Václav, Lynch, William P, Schachner, Melitta, Snyder, Evan Y, 2002. Neural stem cells display an inherent mechanism for rescuing dysfunctional neurons. Nat. Biotechnol. 20 (11), 1103–1110. https://doi.org/10.1038/nbt750.

Pirkmajer, Sergej, Chibalin, Alexander V., 2011. Serum starvation: caveat emptor. Am. J. Physiol. - Cell Physiol. 301 (2), 272–279. https://doi.org/10.1152/ajpcell.00091.2011.

Rabenstein, Monika, Hucklenbroich, Joerg, Willuweit, Antje, Ladwig, Anne, Fink, Gereon Rudolf, Schroeter, Michael, Langen, Karl-Josef, Rueger, Maria Adele, 2015. Osteopontin mediates survival, proliferation and migration of neural stem cells through the chemokine receptor CXCR4. Stem Cell Res. Ther. 6 (1), 99. https://doi.org/10.1186/s13287-015-0098-x.

Rothenberg, Daniel A., Matthew Taliaferro, J., Huber, Sabrina M., Begley, Thomas J., Dedon, Peter C., White, Forest M., 2018. A proteomics approach to profiling the temporal translational response to stress and growth. IScience 9, 367–381. https://doi.org/10.1016/j.isci.2018.11.004.

Ryu, Jae K, Kim, Jean, Cho, Sung J, Hatori, Kozo, Nagai, Astushi, Choi, Hyun B, Lee, Min C, McLarnon, James G, Kim, Seung U, 2004. Proactive transplantation of human neural stem cells prevents degeneration of striatal neurons in a rat model of huntington disease. Neurobiol. Dis. 16 (1), 68–77. https://doi.org/10.1016/J.NBD.2004.01.016.

Shahdadfar, Aboulghassem, Frønsdal, Katrine, Haug, Terje, Reinholt, Finn P., Brinchmann, Jan E., 2005. In vitro expansion of human mesenchymal stem cells: choice of serum is a determinant of cell proliferation, differentiation, gene expression, and transcriptome stability. Stem Cells 23 (9), 1357–1366. https://doi.org/10.1634/stemcells.2005-0094.

Shen, Faping, Song, Chunyan, Liu, Yunmian, Zhang, Jing, Song, Sonya Wei, 2019. IGFBP2 promotes neural stem cell maintenance and proliferation differentially associated with glioblastoma subtypes. Brain Res. 1704 (February), 174–186. https://doi.org/10.1016/J.BRAINRES.2018.10.018.

Shin, Jaehoon, Berg, Daniel A., Zhu, Yunhua, Shin, Joseph Y., Song, Juan, Bonaguidi, Michael A., Enikolopov, Grigori, et al., 2015. Single-cell RNA-seq with waterfall reveals molecular cascades underlying adult neurogenesis. Cell Stem Cell 17 (3), 360–372. https://doi.org/10.1016/j.stem.2015.07.013.

Shinoda, Kosaku, Tomita, Masaru, Ishihama, Yasushi, 2009. EmPAI Calc-for the estimation of protein abundance from large-scale identification data by liquid chromatography-tandem mass spectrometry. Bioinformatics 26 (4), 576–577. https://doi.org/10.1093/bioinformatics/btp700.

Skalnikova, Helena, Motlik, Jan, Gadher, Suresh Jivan, Kovarova, Hana, 2011. Mapping of the secretome of primary isolates of mammalian cells, stem cells and derived cell lines. Proteomics 11 (4), 691–708. https://doi.org/10.1002/pmic.201000402.

Tang, Changyong, Wang, Min, Wang, Peijian, Wang, Lei, Qingfeng, Wu., Guo, Weixiang, 2019. Neural stem cells behave as a functional niche for the maturation of newborn neurons through the secretion of PTN. Neuron 101 (1), 32–44.e6. https://doi.org/10.1016/j.neuron.2018.10.051.

Teixeira, Fábio, Salgado, António, 2020. Mesenchymal stem cells secretome: current trends and future challenges. Neural Regener. Res. 15 (1), 75–77. https://doi.org/10.4103/1673-5374.264455.

Wernly, Bernhard, Gonçalves, Inês, Kiss, Attila, Paar, Vera, Mösenlechner, Tobias, Leisch, Michael, Santer, David, et al., 2017. Differences in stem cell processing lead to distinct secretomes secretion-implications for differential results of previous clinical trials of stem cell therapy for myocardial infarction. Biotechnol. J. 12 (9), 1600732. https://doi.org/10.1002/biot.201600732.

Yasuhara, Takao, Matsukawa, Noriyuki, Hara, Koichi, Guolong, Yu., Lin, Xu., Maki, Mina, Kim, Seung U., Borlongan, Cesario V., 2006. Transplantation of human neural stem cells exerts neuroprotection in a rat model of Parkinson's Disease. J. Neurosci. 26 (48), 12497–12511. https://doi.org/10.1523/JNEUROSCI.3719-06.2006.

Zhao, Sheng, Fernald, Russell D., 2005. Comprehensive algorithm for quantitative real-time polymerase chain reaction. J. Comput. Biol. 12 (8), 1047–1064. https://doi.org/10.1089/cmb.2005.12.1047.

Zheng, Grace X.Y., Terry, Jessica M., Belgrader, Phillip, Ryvkin, Paul, Bent, Zachary W., Wilson, Ryan, Ziraldo, Solongo B., et al., 2017. Massively parallel digital transcriptional profiling of single cells. Nature Commun. https://doi.org/10.1038/ncomms14049.

Zhou, Yi, Bond, Allison M, Shade, Jamie E, Zhu, Yunhua, Davis, Chung-Ha O, Wang, Xinyuan, Yijing, Su., et al., 2018. Autocrine Mfge8 signaling prevents developmental exhaustion of the adult neural stem cell pool. Cell Stem Cell 23 (3), 444–452.e4. https://doi.org/10.1016/j.stem.2018.08.005.

Zywitza, Vera, Misios, Aristotelis, Bunatyan, Lena, Willnow, Thomas E, Rajewsky, Nikolaus, 2018. Single-cell transcriptomics characterizes cell types in the subventricular zone and uncovers molecular defects impairing adult neurogenesis. Cell Rep. 25 (9), 2457–2469.e8. https://doi.org/10.1016/j.celrep.2018.11.003.